

Highlights

Progressive self-supervised blind-spot denoising method for LDCT denoising

Yichao Liu, Yueyang Teng, Junwen Guo

- a progressive self-supervised blind-spot denoising framework is proposed for LDCT that requires only low-dose CT images and no paired normal-dose data.
- The step-wise masking and denoising strategy enables fine-grained noise suppression and effectively bridges the performance gap between self-supervised and supervised methods.
- A noise-based regularization mechanism, implemented by injecting controlled noise into both inputs and targets, effectively mitigates overfitting and strengthens the self-supervised learning signal.
- Extensive experiments demonstrate architecture-agnostic performance improvements, with results comparable to or surpassing representative supervised LDCT denoising methods.

Progressive self-supervised blind-spot denoising method for LDCT denoising

Yichao Liu^a, Yueyang Teng^{b,c,*}, Junwen Guo^{d,*}

^a*IWR, Heidelberg University, Heidelberg, 69120, Baden Württemberg, Germany*

^b*College of Medicine and Biological Information Engineering, Northeastern University, Shenyang, 110169, Liaoning, China*

^c*Key Laboratory of Intelligent Computing in Medical Image, Ministry of Education, Shenyang, 110169, Liaoning, China*

^d*Department of Epidemiology & Global Health, Umeå University, , Umeå, 90187, Sweden*

Abstract

Self-supervised learning is increasingly investigated for low-dose computed tomography (LDCT) image denoising, as it alleviates the dependence on paired normal-dose CT (NDCT) data, which are often difficult to acquire in clinical practice. In this paper, we propose a novel self-supervised training strategy that relies exclusively on LDCT images. We introduce a step-wise blind-spot denoising mechanism that enforces conditional independence in a progressive manner, enabling more fine-grained denoising learning. In addition, we add Gaussian noise to LDCT images, which acts as a regularization and mitigates overfitting. Extensive experiments on the Mayo LDCT dataset demonstrate that the proposed method consistently outperforms existing self-supervised approaches and achieves performance comparable to, or better than, several representative supervised denoising methods.

Keywords: Self-supervised learning, LDCT denoising, Progressive learning, Blind spot denoising

*Corresponding author

Email addresses: tengyy@bime.neu.edu.cn (Yueyang Teng), junwen.guo@umu.se (Junwen Guo)

1. Introduction

Low-dose computed tomography (LDCT) plays a critical role in reducing radiation exposure to patients while maintaining diagnostic utility, in accordance with the “as low as reasonably achievable” (ALARA) principle [1]. However, lowering the radiation dose inevitably increases noise and artifacts in reconstructed CT images, which can severely degrade image quality and hinder accurate clinical interpretation. To address this issue, image denoising has become an essential post-processing step in LDCT imaging pipelines, aiming to suppress noise while preserving diagnostically relevant anatomical structures.

Extensive efforts have been devoted to LDCT image denoising in recent years. Supervised learning-based approaches remain the dominant paradigm and have achieved strong performance. Representative methods include convolutional neural network (CNN)-based models such as U-Net [2], Residual Encoder-Decoder CNN (RED-CNN) [3], and cycle-consistent generative adversarial networks (CycleGANs) [4, 5], Transformer-based architectures such as CTformer [6], as well as hybrid models combining convolution and attention mechanisms, for example, Swin-UNet [7].

However, traditional LDCT denoising methods depend heavily on paired normal-dose CT (NDCT) images, which are often scarce in clinical practice. With the advancement of deep learning, unsupervised approaches, particularly self-supervised learning, have gained increasing attention due to their ability to learn without clean references. Classical model-based methods like Block-Matching 3D (BM3D) [8] suppress noise by exploiting non-local self-similarity through grouping similar patches and performing collaborative filtering in a transform domain. More recently, self-supervised learning techniques, collectively known as Noise2- methods, have substantially advanced denoising performance by leveraging different assumptions about noise and data availability. Noise2Noise [9] trains a network to map one noisy observation to another under the assumption that noise realizations are independent and zero-mean, thus requiring multiple noisy instances of the same image but no clean targets. Noise2Self [10] relaxes this requirement by formalizing a conditional independence assumption, training networks to predict each pixel exclusively from its spatial neighbors. This allows effective denoising using only single noisy images, without clean targets or paired noisy data. Building on this framework, Noise2Void [11] further introduces a masking strategy in which selected pixels are predicted from their surrounding con-

text, relying on the assumptions that noise is independent across pixels and that the underlying signal can be inferred from neighboring pixels. In contrast, Neighbor2Neighbor [5] avoids explicit masking and instead assumes that neighboring patches share the same underlying clean signal but contain different noise realizations, enabling one noisy patch to supervise the denoising of the other.

Building upon the core assumptions underlying Noise2Noise, Noise2Void, and Noise2Self, a series of extensions have been proposed to relax data requirements or strengthen training constraints in self-supervised denoising. Noise2Inverse [12] extends the Noise2Noise paradigm to tomographic imaging by splitting a single raw sinogram into independent subsets of projection angles, producing multiple noisy reconstructions of the same anatomy. Under the assumption of independent measurement noise and identical underlying structure, the network learns to suppress noise by predicting one reconstruction from another. Noise2Same [13] addresses the information loss introduced by blind-spot masking through a dual-forward pass strategy, enforcing consistency between masked and unmasked predictions and thereby improving detail preservation over earlier methods such as Noise2Void. From a probabilistic perspective, Noise2Score [14] formulates self-supervised denoising as a Bayesian score estimation problem, learning the gradient of the log-probability density directly from noisy data without clean references; the clean image is then analytically recovered via Tweedie’s formula, enabling a unified treatment of noise from the exponential family, including Gaussian and Poisson distributions. In a complementary direction, Noise2Sim [15] exploits structural similarity across intrinsically registered sub-images, such as adjacent CT slices, and uses them as training pairs to suppress both independent and correlated noise. Under the assumption that noise and structural discrepancies between similar sub-images are zero-mean, Noise2Sim is theoretically shown to be asymptotically equivalent to supervised Noise2Clean training.

In this paper, inspired by the observation of Zhu *et al.* [16] that the transformation from low-quality LDCT images to high-quality NDCT images can be progressively approximated by neural networks, we propose a progressive self-supervised learning framework for LDCT image denoising. Building on the blind-spot denoising principle, the proposed approach extends it in a step-wise manner, allowing the network to progressively improve image quality by denoising inputs in a more fine-grained way. To further mitigate overfitting, we add random noise of identical intensity to both input and tar-

get images. Extensive experiments demonstrate that the proposed method consistently outperforms existing self-supervised denoising approaches and achieves performance competitive with, or superior to, some representative supervised methods.

2. Methodology

This section introduces the proposed progressive self-supervised denoising method, which extends the blind-spot method by incorporating a step-wise masking scheme.

2.1. Supervised noise2clean

We first consider LDCT denoising in a supervised learning setting. Given a LDCT image x_i and the corresponding NDCT image y_i , assuming $x = x_c + n_0$, the denoising process can be expressed as:

$$\operatorname{argmin}_{\theta} \sum_i L(f_{\theta}(x_i), y_i) \quad (1)$$

where, x_c is the clean CT images and n_0 is the noise on LDCT images, f_{θ} represents denoising networks with optimal parameters θ , and L denotes the loss function. By assuming that the noise is zero-mean and independent across all dimensions, self-supervised learning methods such as Noise2Self can be developed.

2.2. Noise2Self

Noise2Self is trained using the loss function $\mathcal{L}(f) = E_x \|f(x) - x\|^2$. Importantly, the function f is required to be \mathcal{J} -invariant, as established by Batson *et al.* [10] to prevent learning the identity mapping. Thanks to \mathcal{J} -invariant and the zero-mean assumption of noise, minimizing the self-supervised loss $E_x \|f(x) - x\|^2$ indirectly minimizes the supervised loss $E_x \|f(x) - y\|^2$ [13], which can be expressed as:

$$E_x \|f(x) - x\|^2 \propto E_x \|f(x) - y\|^2 \quad (2)$$

Currently, all existing implementations for computing the \mathcal{J} -invariant denoising function f rely on blind-spot networks [11, 10, 17].

2.3. Progressive self-supervised denoising

Consider a temporal supervised denoising process where \hat{x}_t denotes the denoised LDCT image at time t and $\text{noise}(t)$ represents the noise at time t . The output denoised image \hat{x}_t serves as the input for the next time step, such that $f(\hat{x}_t) = \hat{x}_{t+1}$. The denoising process is illustrated as follows:

$$\begin{aligned}\hat{x}_t &= f(\hat{x}_t) + \text{noise}(t), \hat{x}_{t+1} = f(\hat{x}_{t+1}) + \text{noise}(t+1) \\ &\dots, \hat{x}_{t+n} = f(\hat{x}_{t+n}) + \text{noise}(t+n)\end{aligned}\quad (3)$$

As the time step t increases, \hat{x}_t should progressively approach the NDCT image y .

$$\lim_{t \rightarrow \infty} \hat{x}_t = \lim_{t \rightarrow \infty} f(\hat{x}_t) = y, \lim_{t \rightarrow \infty} \text{noise}(t) = 0 \quad (4)$$

Since minimizing the self-supervised loss $E_x \|f(x) - x\|^2$ indirectly minimizes the supervised loss $E_x \|f(x) - y\|^2$, the $\lim_{t \rightarrow \infty} \text{noise}(t) = 0$ should also hold for $E_x \|f(x) - x\|^2$ as well. Therefore, a step-wise blind-spot self-supervised loss function can be formulated as follows:

$$\operatorname{argmin}_{\theta} \sum_i L(f_{\theta}(M \odot \hat{x}_i^t), x_i) \quad (5)$$

Where $M \sim \mathcal{M}_{\alpha}\{M_1, \dots, M_n\}$ is a binary random mask. \mathcal{M}_{α} denotes a set of masks with random sampling rate α . \odot represents the Hadamard (element-wise) product. Here, Similar to supervised temporal denoising, the update is given by $\hat{x}_i^{t+1} = f_{\theta}(M \odot \hat{x}_i^t)$

To prevent overfitting and encourage the model to learn contextual features rather than noise, we add random zero-mean noise n_1 to the input x_i and n_2 to the target x_i . Note that this does not violate Eq. (2). As detailed in the following,

$$E_x \|f(x + n_1) - (x + n_2)\|^2 = E_{x,y} \|f(x + n_1) - (y + n_2)\|^2 \quad (6)$$

$$+ E_{x,y} \|x - y\|^2 - 2\langle f(x + n_1) - (y + n_2), x - y \rangle \quad (7)$$

$$= E_{x,y} \|f(x + n_1) - (y + n_2)\|^2 + E_{x,y} \|x - y\|^2 \quad (8)$$

Here, since f is \mathcal{J} -invariant and the zero-mean noise assumption holds, minimizing Eq. (8) indirectly minimizes $E_x \|f(x) - y\|^2$.

Therefore, the final loss function is defined as follows:

$$\operatorname{argmin}_{\theta} \sum_i L(f_{\theta}(M \odot (\hat{x}_i^t + \mathbb{1}_{\{\hat{x}_i^t=x\}} n_1), x_i + n_2)) \quad (9)$$

Where $\mathbb{1}_{\{\hat{x}_i^t=x\}}$ is the indicator function that equals one when the input is an LDCT image. In this work, we generate n_1 and n_2 as a combination of Poisson noise and additive white Gaussian noise (AWGN) [16].

The advantage of our method is that it requires only LDCT images for training. At each denoising time step, a random mask is applied and the model is optimized by minimizing Eq. (5). Intuitively, this random masking strategy progressively suppresses noise-corrupted pixels, enabling the model to recover the underlying anatomical structures and contextual information of the CT image over k denoising steps. During inference, we sample k differently masked versions of the LDCT image, and the final denoised CT image is obtained by averaging the corresponding outputs. An overview of the proposed progressive self-supervised denoising framework is shown in Fig. 1.

3. Experiments

We first introduce the configuration of dataset and experiments. We discuss the progressive blind-spot strategy and noise configurations through ablation experiments. We also experimentally verify the generalizability of the model for different patients. Finally, we compare our method to several supervised and self-supervised methods.

3.1. Experimental details

We conduct our experiments on the AAPM Low-Dose CT Grand Challenge dataset, a publicly available benchmark that provides paired low-dose and standard-dose CT scans acquired under identical imaging conditions [18]. The dataset includes scans from multiple anatomical regions. Each volume is reconstructed with an in-plane resolution of 512×512 and a voxel spacing of $0.5859 \times 0.5859 \times 3.0 \text{ mm}^3$. A total of 36 subjects are included, with 27 volumes used for training and the remaining 9 reserved for testing to ensure subject-level separation. All images are provided in DICOM format and are first converted to Hounsfield Units (HU) to preserve the physical meaning of CT attenuation values. The intensities are then normalized to the range $[0, 1]$ using a fixed HU window of $[-1024, 3072]$, which covers air, soft tissue,

and high-density structures while maintaining consistency across subjects and experiments. It is worth noting our method does not require any NDCT at the training stage.

We implemented our model using the PyTorch 2.7 library and trained it on a server equipped with a single NVIDIA V100 GPU. The Adam optimizer was employed with parameters $\beta_1 = 0.9$, $\beta_2 = 0.99$, and $\epsilon = 10^{-8}$. The initial learning rate was set to 10^{-3} and decayed by a factor of two every 20 epochs. Training was conducted for a total of 100 epochs. We used a batch size of 1, with 10 patches per image and a patch size of 128×128 . The combination noise with zero mean and variance 10 of AWGN was added to both the network inputs and targets.

For quantitative assessment, model performance is evaluated using three widely adopted image quality metrics: peak signal-to-noise ratio (PSNR), structural similarity index (SSIM), and root mean squared error (RMSE). These metrics are computed in accordance with the evaluation protocol described in Chen *et al.* [3], enabling consistent and reproducible comparison across methods. PSNR and RMSE quantify pixel-wise fidelity between the denoised and reference images, while SSIM measures structural and perceptual similarity. The mathematical formulation shows as Eq. 10 and Eq. 11. We use the standard deviation as a measure of variability to assess the stability of the models.

$$PSNR = 10 \log_{10} \left(\frac{MAX^2}{\frac{1}{n} \sum_{i=1}^n (m_i - l_i)^2} \right) \quad (10)$$

where m_i and l_i are pixels of LDCT or denoised CT images and NDCT images, respectively. n is the number of pixels in the image and MAX denotes the maximum value of the image pixels.

$$SSIM(m, l) = \frac{(2\mu_m\mu_l + c_1)(\sigma_{ml} + c_2)}{(\mu_m^2 + \mu_l^2 + c_1)(\sigma_m^2 + \sigma_l^2 + c_2)} \quad (11)$$

where μ_m and μ_l are the means of m and l , respectively; σ_m^2 and σ_l^2 are variances of m and l , respectively. σ_{ml} is the covariance of m and l , and c_1 and c_2 are two hyperparameters for stabilizing the division operation.

3.2. Results

3.2.1. Number of time steps

The number of time steps k was selected empirically through a number of experiments. To ensure consistency between training and inference, the

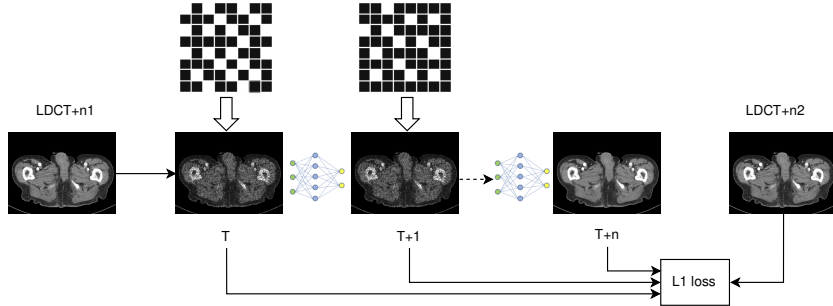


Figure 1: Overview of progressive self-supervised denoising method

number of mask sampling steps during inference was also set to k . We evaluated k in the range of 1 to 6. As shown in Fig. 2, the denoising performance consistently improves as k increases and reaches its optimum at $k = 5$. Further increasing k leads to a degradation in performance in both PSNR and SSIM.

This indicates that from 1 step to 5 steps, the model learns to gradually denoise. Such behavior is expected, as accurate recovery of corrupted regions requires sufficient contextual information from other parts of the image, which cannot be fully propagated in a single denoising step. By iteratively applying the denoising process, the model progressively refines its predictions and aggregates increasingly global contextual cues, leading to improved reconstruction quality. This observation is consistent with the trend shown in Fig. 2, where performance improves with increasing k until sufficient contextual information has been accumulated.

3.2.2. Noise level

To investigate the impact of noise level on model performance, we evaluate different levels of the combination noise, parameterized by the standard deviation of the Gaussian distribution. Fig. 3 illustrates the effect of varying noise levels on performance over the test set. As the noise variance increases, both PSNR and SSIM consistently decrease, indicating degraded reconstruction quality. The highest PSNR is achieved at a noise level of 10. For SSIM, the differences among noise levels 5, 10, and 15 are relatively minor, suggesting limited sensitivity within this range.

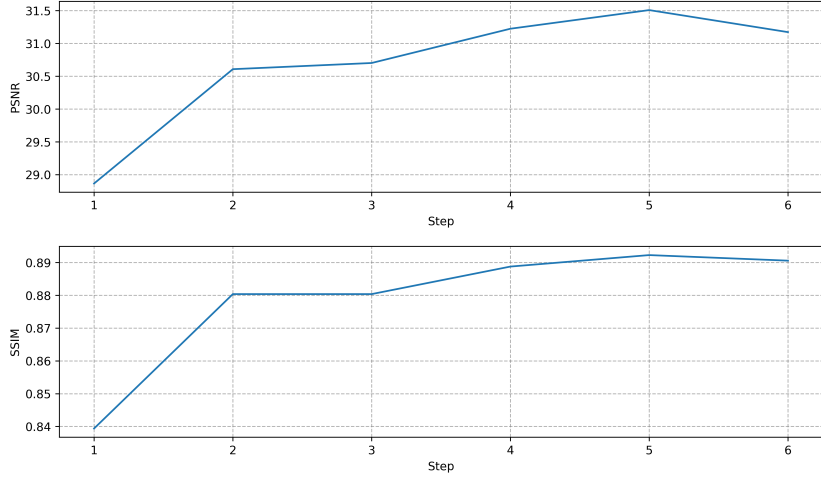


Figure 2: Quantitative results on the test set: number of time steps

3.2.3. Mask ratio

We perform point-wise Bernoulli sampling over the spatial domain, where each pixel is independently activated with a success probability α , corresponding to the masking ratio. Fig. 4 summarizes the impact of different masking ratios on denoising performance.

PSNR reaches its maximum at $\alpha = 0.1$, while SSIM seems remains relatively stable over a broad range of masking ratios from $\alpha = 0.01$ to $\alpha = 0.2$. When the masking ratio is too low ($\alpha = 0.1$), the supervision signal remains weak due to the high similarity between input and target, limiting performance improvements. Conversely, excessively high masking ratios ($\alpha = 0.2$) removes substantial contextual information, resulting in degraded reconstruction quality and reduced structural fidelity.

3.2.4. ablation study

We further conducted ablation experiments to analyze the effects of combining Poisson and AWGN with the proposed progressive self-supervised blind-spot strategy. The results are summarized in Table 1.

As shown, applying the progressive self-supervised blind-spot strategy alone yields only marginal performance improvements compared to the LDCT baseline reported in Table 2. This is primarily because the input and target images remain largely identical, which limits the learning signal and leads to overfitting. In contrast, introducing noise substantially enhances per-

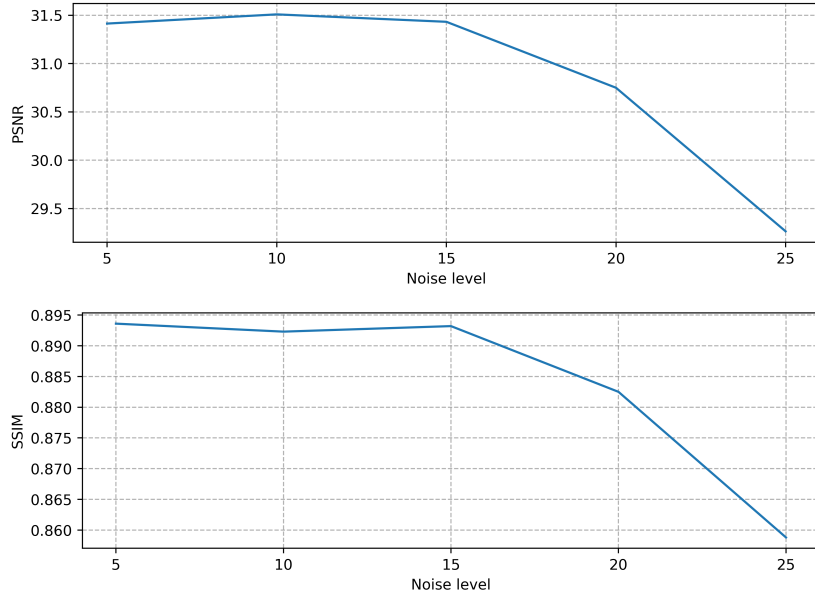


Figure 3: Quantitative results on the test set: variance level of combination noise

Metric	w combination noise	w progressive masked denoise	w both
PSNR	30.242	29.143	31.510
SSIM	0.877	0.863	0.892
RMSE	12.718	14.488	10.993

Table 1: Results of ablation study for both combination noise and progressive masked denoise strategy. 'w' represents 'with'.

formance by increasing the discrepancy between input and target, thereby encouraging the model to learn more robust and meaningful denoising representations.

3.2.5. patient analysis

We further evaluate the stability of our method across different patients. Fig. 5 presents a quantitative comparison between LDCT and our method in terms of PSNR, SSIM, and RMSE. The results demonstrate that our method exhibits substantially lower variance than LDCT, particularly for SSIM and RMSE, indicating more consistent reconstruction quality across patients. Moreover, our method consistently outperforms LDCT for all evaluated patients, including cases where the LDCT images already achieve rel-

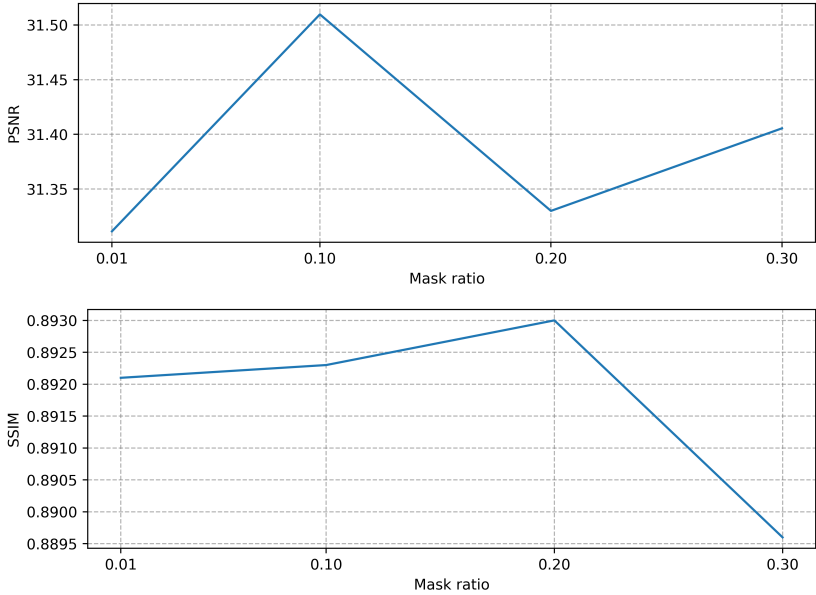


Figure 4: Quantitative results on the test set: Mask ratio for progressive self-supervised denoising

atively high PSNR values.

3.2.6. Method comparison

We compared our method with several representative supervised and unsupervised approaches, including RED-CNN [3], Swin-Unet [7], CycleGAN [4], BM3D [8], Noise2Void [11], and Neighbor2Neighbor [19]. Among these, RED-CNN, Swin-Unet, and CycleGAN were trained in a supervised manner, whereas the remaining methods were trained solely on LDCT images. Except for BM3D and RED-CNN, all learning-based baselines adopt a U-Net or U-Net-based backbone. It is worth noting that, unlike Noise2Self, operates on a standard U-Net architecture with batch normalization instead of instance normalization.

Table 2 reports the quantitative comparison on the LDCT dataset. It can be clearly observed that our method consistently outperforms commonly used self-supervised denoising approaches across all evaluation metrics. In particular, the proposed progressive self-supervised blind-spot denoising with U-Net not only surpasses unsupervised baselines but also outperforms certain supervised methods, such as Cycle-GAN, and achieves performance compa-

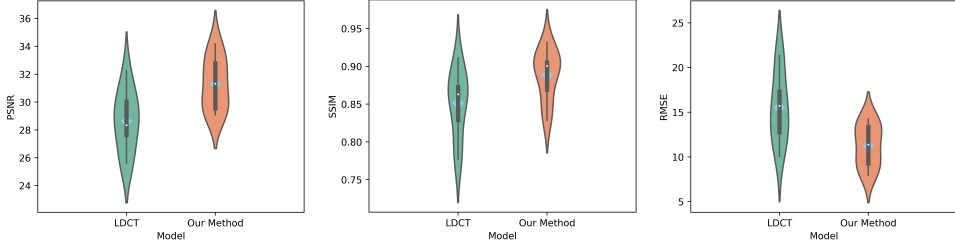


Figure 5: Quantitative results on the test set of different patients

Methods	PSNR	SSIM	RMSE	parameters
LDCT	28.842	0.856	15.160	-
RED-CNN	31.748	0.896	10.686	1.85M
Swin-Unet	31.060	0.890	11.558	0.95M
Cycle GAN	30.289	0.879	12.813	114M
BM3D	29.103	0.842	14.281	-
Noise2Void	29.489	0.864	14.014	31M
Neighbor2Neighbor	30.078	0.876	13.099	31M
ours+Unet	31.510	0.892	10.993	31M
ours+Swin-Unet	30.570	0.881	12.134	0.95M
ours+RED-CNN	31.261	0.889	11.324	1.85M

Table 2: Quantitative evaluation for LDCT dataset.

rable to the widely adopted supervised approach RED-CNN.

Similar performance gains are observed when integrating the proposed method with Swin-Unet and RED-CNN backbones. In these cases, our self-supervised models exhibit performance close to their corresponding supervised counterparts, demonstrating that the proposed strategy is architecture-agnostic and can effectively enhance denoising performance without introducing additional model complexity.

We further demonstrate the effectiveness of the proposed method on a representative pelvis slice, as shown in Fig. 6. The proposed approach achieves superior noise suppression while preserving sharp anatomical boundaries and fine structural details, yielding results that are visually closest to the FDCT reference. In contrast, other methods, particularly self-supervised approaches, as well as certain supervised models such as Swin-Unet and Cycle-GAN, exhibit noticeable residual noise or introduce smoothing artifacts that degrade structural fidelity. This demonstrates that our progressive

self-supervised denoising strategy effectively balances noise removal and detail preservation without relying on paired NDCT data.

4. Conclusions

In this paper, we proposed a progressive self-supervised blind-spot denoising framework for LDCT imaging that relies exclusively on LDCT data and does not require paired NDCT images during training. By extending the conventional blind-spot self-supervised paradigm into a step-wise denoising process, the proposed method enables the network to progressively suppress noise and refine image quality in a more fine-grained manner. In addition, introducing controlled random noise to both inputs and targets acts as an effective regularization strategy, mitigating overfitting and strengthening the self-supervised learning signal.

Extensive experiments on the AAPM LDCT dataset demonstrate that the proposed method consistently outperforms existing self-supervised denoising approaches across multiple quantitative metrics, including PSNR, SSIM, and RMSE. Notably, the proposed framework achieves performance comparable to, and in some cases exceeding, representative supervised methods such as RED-CNN and Cycle-GAN. Qualitative results further confirm that our method effectively suppresses noise while preserving fine anatomical structures, producing reconstructions that are visually close to FDCT references. Moreover, the method exhibits strong robustness across different patients, indicating stable and reliable denoising performance.

An important advantage of the proposed approach is its architecture-agnostic nature. By integrating the progressive self-supervised strategy with different backbone networks, including U-Net, Swin-Unet, and RED-CNN, we observe consistent performance improvements without increasing model complexity. This highlights the general applicability of the proposed framework and its potential for seamless integration into existing LDCT denoising pipelines.

Overall, this work demonstrates that progressive self-supervised learning is a powerful alternative to conventional one-step denoising strategies and provides an effective solution for LDCT denoising in scenarios where paired clean data are unavailable. Future work will explore extending the proposed framework to other imaging modalities, incorporating adaptive step scheduling, and further validating its clinical impact on downstream diagnostic tasks.

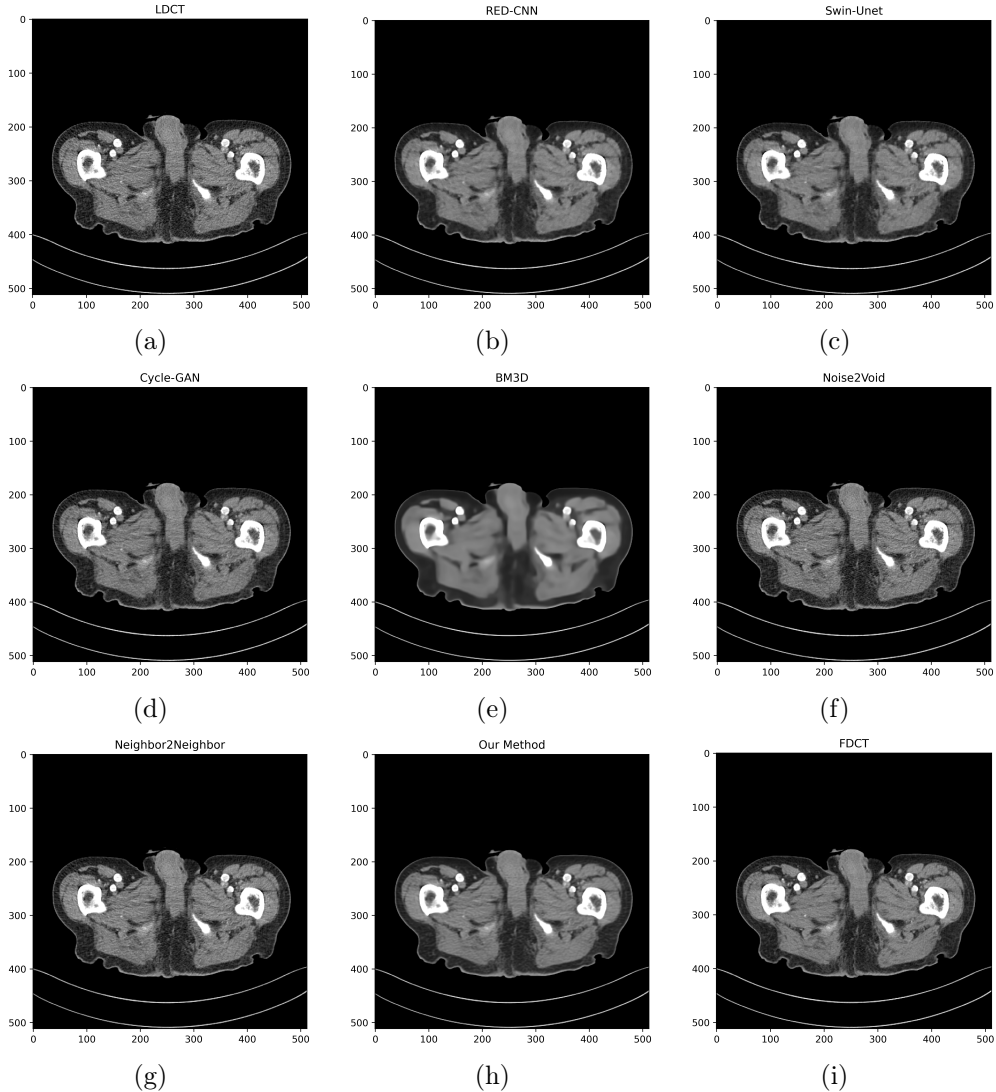


Figure 6: Results of pelvis image for comparison. (a)LDCT, (b)RED-CNN,(c)Swin-Unet, (d)Cycle-GAN, (e)BM3D, (f)Noise2Void, (g)Neighbor2Neighbor, (h)Ours, (I)FDCT

Appendix A. Example Appendix Section

References

- [1] R. Smith-Bindman, J. Lipson, R. Marcus, K.-P. Kim, M. Mahesh, R. Gould, A. B. De González, D. L. Miglioretti, Radiation dose associated with common computed tomography examinations and the associated lifetime attributable risk of cancer, *Archives of internal medicine* 169 (22) (2009) 2078–2086.
- [2] O. Ronneberger, P. Fischer, T. Brox, U-net: Convolutional networks for biomedical image segmentation, in: International Conference on Medical image computing and computer-assisted intervention, Springer, 2015, pp. 234–241.
- [3] H. Chen, Y. Zhang, M. K. Kalra, F. Lin, Y. Chen, P. Liao, J. Zhou, G. Wang, Low-dose ct with a residual encoder-decoder convolutional neural network, *IEEE transactions on medical imaging* 36 (12) (2017) 2524–2535.
- [4] J.-Y. Zhu, T. Park, P. Isola, A. A. Efros, Unpaired image-to-image translation using cycle-consistent adversarial networks, in: Proceedings of the IEEE international conference on computer vision, 2017, pp. 2223–2232.
- [5] Z. Li, J. Huang, L. Yu, Y. Chi, M. Jin, Low-dose ct image denoising using cycle-consistent adversarial networks, in: 2019 IEEE nuclear science symposium and medical imaging conference (NSS/MIC), IEEE, 2019, pp. 1–3.
- [6] D. Wang, F. Fan, Z. Wu, R. Liu, F. Wang, H. Yu, Ctformer: convolution-free token2token dilated vision transformer for low-dose ct denoising, *Physics in Medicine & Biology* 68 (6) (2023) 065012.
- [7] H. Cao, Y. Wang, J. Chen, D. Jiang, X. Zhang, Q. Tian, M. Wang, Swin-unet: Unet-like pure transformer for medical image segmentation, in: European conference on computer vision, Springer, 2022, pp. 205–218.
- [8] K. Dabov, A. Foi, V. Katkovnik, K. Egiazarian, Image denoising by sparse 3-d transform-domain collaborative filtering, *IEEE Transactions on image processing* 16 (8) (2007) 2080–2095.

- [9] J. Lehtinen, J. Munkberg, J. Hasselgren, S. Laine, T. Karras, M. Aittala, T. Aila, Noise2noise: Learning image restoration without clean data, arXiv preprint arXiv:1803.04189 (2018).
- [10] J. Batson, L. Royer, Noise2self: Blind denoising by self-supervision, in: International conference on machine learning, PMLR, 2019, pp. 524–533.
- [11] A. Krull, T.-O. Buchholz, F. Jug, Noise2void-learning denoising from single noisy images, in: Proceedings of the IEEE/CVF conference on computer vision and pattern recognition, 2019, pp. 2129–2137.
- [12] A. A. Hendriksen, D. M. Pelt, K. J. Batenburg, Noise2inverse: Self-supervised deep convolutional denoising for tomography, IEEE Transactions on Computational Imaging 6 (2020) 1320–1335.
- [13] Y. Xie, Z. Wang, S. Ji, Noise2same: Optimizing a self-supervised bound for image denoising, Advances in neural information processing systems 33 (2020) 20320–20330.
- [14] K. Kim, J. C. Ye, Noise2score: tweedie’s approach to self-supervised image denoising without clean images, Advances in Neural Information Processing Systems 34 (2021) 864–874.
- [15] C. Niu, M. Li, F. Fan, W. Wu, X. Guo, Q. Lyu, G. Wang, Noise suppression with similarity-based self-supervised deep learning, IEEE transactions on medical imaging 42 (6) (2022) 1590–1602.
- [16] Y. Zhu, Q. He, Y. Yao, Y. Teng, Self-supervised noise2noise method utilizing corrupted images with a modular network for ldct denoising, Pattern Recognition 161 (2025) 111285.
- [17] S. Laine, T. Karras, J. Lehtinen, T. Aila, High-quality self-supervised deep image denoising, Advances in neural information processing systems 32 (2019).
- [18] T. R. Moen, B. Chen, D. R. Holmes III, X. Duan, Z. Yu, L. Yu, S. Leng, J. G. Fletcher, C. H. McCollough, Low-dose ct image and projection dataset, Medical physics 48 (2) (2021) 902–911.

- [19] T. Huang, S. Li, X. Jia, H. Lu, J. Liu, Neighbor2neighbor: Self-supervised denoising from single noisy images, in: Proceedings of the IEEE/CVF conference on computer vision and pattern recognition, 2021, pp. 14781–14790.